The manuscript by Saini et al. is a continuation of a series of works where the effect of glacial-interglacial changes on planktic functional types and the carbon cycle is explored. Here they focus on differences between a portion of the onset of the last glaciacion (70 ky) and the Holocene. In particular the effect of different surface iron fluxes to the ocean on atmospheric CO2 and global ocean DIC is tested. The manuscript is clearly written. I have some comments regarding the methodology and presentation of results that should be addressed for the paper to be published by Climate of the Past.

We thank Dr Muglia for his helpful feedback on our manuscript. Please find below answers to the comments raised.

Black: Reviewer's comments.
Red: Author's responses
Green: Modified text in the manuscript.

In the methodology, the authors give an analysis of different estimates of iron from dust solubilities, and they define a "most likely range" between 3 and 5%. Is this estimate also valid for preindustrial dust? For your preindustrial simulation you pragmatically chose 1% solubility. The estimate of CO2 effect of Southern Ocean fertilization is based on the comparison of 70 ky simulations that use 3-5 % Fe solubility in the Southern Ocean vs a 70 ky simulation that uses preindustrial iron fluxes with 1% solubility. Due to the high variations in estimates of Fe solubility in the ocean, which the authors correctly point out, I think that the case of same solubility between glacial and interglacials should be included in the "most likely scenarios". This will affect the minimum of your range of CO2 change estimates due to Fe fertilization of the Southern Ocean.

We thank Dr Muglia for this very constructive comment and agree with the suggestion of including estimates of CO_2 drawdown based on the same solubility for glacial and interglacial dust. We have now included five new sensitivity experiments performed under 70 ka background conditions but using a pre-industrial (PI) iron mask with an iron solubility factor ranging between 3% and 20%. This approach allows us to estimate the minimum change in CO_2 drawdown due to glacial dust fluxes, assuming no change in solubility over time. We have included this information in the text as below:

Lines 135-143:

However, due to the uncertainties associated with present-day iron solubilities, we perform additional sensitivity experiments under 70 ka BP boundary conditions using the PI iron dust mask with iron solubility varying between 3% and 20%. This approach allows us to estimate the minimum change in CO_2 due to glacial dust fluxes, assuming no change in solubility over time. The corresponding CO_2 changes can be calculated by taking the difference between CO_2 changes achieved with the full experiments (i.e., changing masks and solubilities) and the CO_2 changes achieved by only changing solubility. This approach was validated by performing two additional 70ka equilibrium experiments with the pife mask and an iron solubility of 3% and 10% from which we branched off simulations with the lambfe mask and constant solubility (not shown). The resulting CO_2 drawdown in these experiments was the same than if calculated as the difference between the full experiments and solubility-only experiments.

The results from these new experiments are now included throughout the manuscript.

Lines 9-10:

If surface water iron solubility is considered constant through time, we find a CO_2 draw-down of ~4 to ~8 ppm.

Lines 198-200:

Changing the iron flux masks from PI to glacial at 70ka BP leads to a 3.8 to 8.3 ppm drop in atmospheric CO_2 concentration if we assume that the mean iron solubility remains unchanged (Table 2). Interestingly, for solubilities of 3% and higher, the drawdown is nearly constant, regardless of the glacial dust flux mask and regardless of the solubility (7.3 ± 1 ppm).

Lines 363-369:

We find that the biological response to changes in iron fertilization not only depends on the iron solubility during glacial periods but also on the iron solubility during warm periods. Our results are based on the assumption that the global average iron solubility during warm periods equals ~1%. At higher initial values, the total potential draw-down of CO_2 would be smaller. For example, for an assumed solubility during warm periods closer to ~3%, we simulate a range of CO_2 changes between 6.4 ppm (no change in solubility and glacial fluxes based on Lambert et al., 2015) and 16.4 ppm (change to 20% solubility and glacial fluxes based on Ohgaito et al., (2018). This range reduces to 6.9-14.4 ppm if the initial solubility was 5% and to 6.7-6.9ppm if the initial solubility was 20%.

However, there is evidence suggesting that iron solubility could have been higher during glacial than interglacial periods (Lines 124-129). We now add the following text:

Lines 129-131:

Iron is more bioavailable in dust that originates from physically weathered than from chemically weathered bedrock (Shoenfelt et al., 2017). The analysis of subantarctic marine sediment cores further suggests that aeolian iron was 15 to 20 times more bioavailable during glacial periods than during the current interglacial (Shoenfelt et al., 2018).

Based on this, we add the following statement:

Line 134:

During warmer climates, such as PI or at the MIS4 onset, we define the most likely solubility factor as 1%.

Therefore, we present a detailed discussion only for experiments that switch from a PI iron mask with 1% solubility to glacial iron masks with 1% and higher solubilities. These changes are also included in Figure 4 (Fig.R1 below) of the manuscript and in Tables 1, 2 and 3.

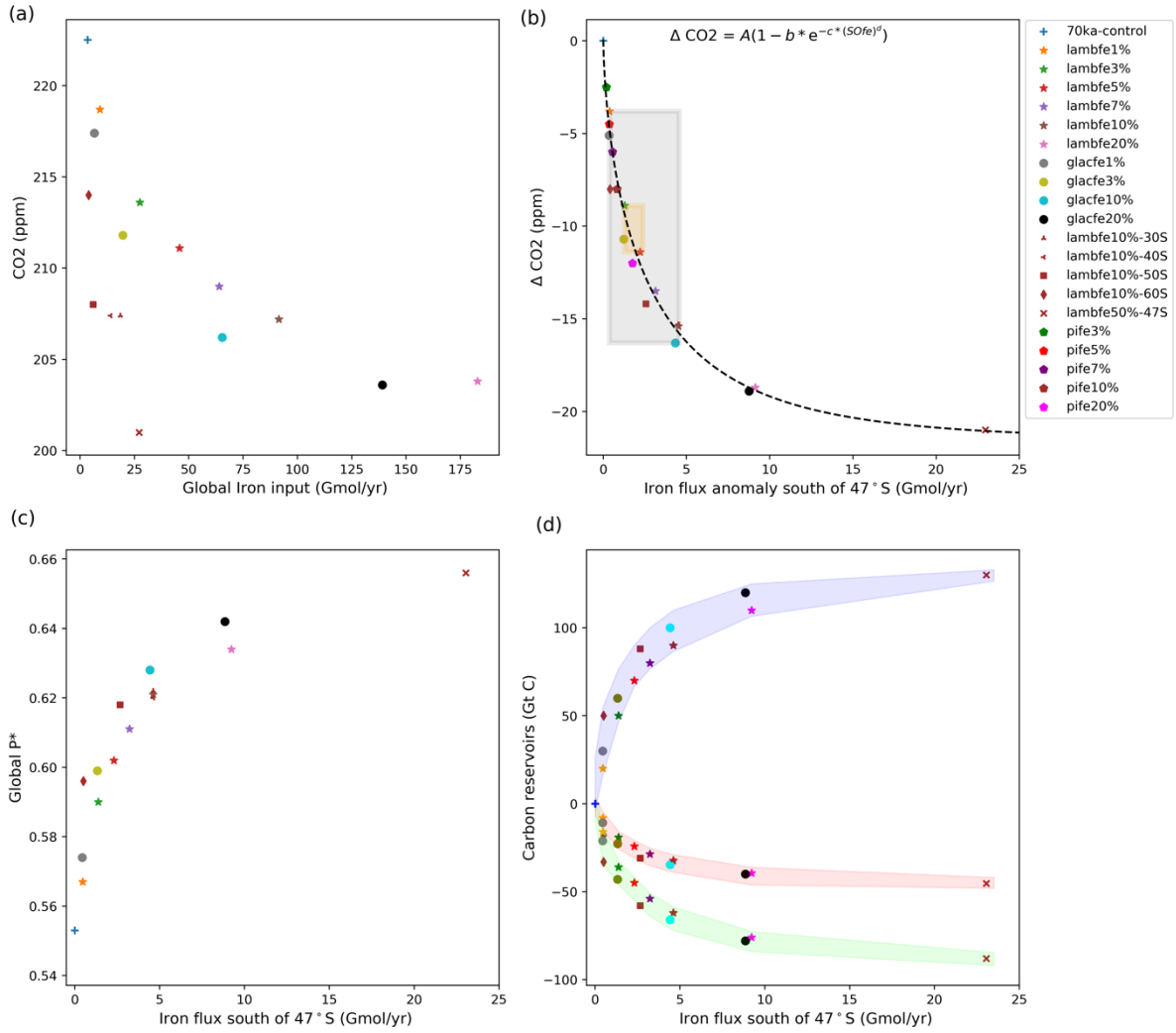

Fig.R1: (a) Equilibrated atmospheric CO_2 concentration (ppm) as a function of the globally integrated aeolian iron flux into the ocean (Gmolyr^{-1}). (b) Atmospheric ΔCO_2 concentration (ppm) as a function of changes in aeolian iron flux into the Southern Ocean south of 47°S. The grey shading represents the range of likely glacial iron solubilities (1-10%) and the associated change in CO_2 concentrations (-4 to -16 ppm), while the orange shading represents our best estimate of change in CO_2 (-9 to -11 ppm) for a solubility of 1% during warm periods and 3-5% during colder periods. Note that lambfe10%, lambfe10%-30S and lambfe10%-40S are overlapping. The black curve represents the best fit and suggests a maximum CO_2 draw-down of ~21 ppm due to Southern Ocean iron fertilisation. (c) Global P^* as a function of aeolian iron flux into the Southern Ocean south of 47°S and (d) Globally integrated carbon reservoirs (GtC) as a function of aeolian iron flux into the Southern Ocean south of 47°S. The shadings represent ocean carbon (blue), atmospheric carbon (red) and terrestrial carbon (green).

Table 1: Aeolian iron fluxes for each experiment.

Experiment	Total iron flux into the ocean ($Gmolyr^{-1}$)	Iron flux into the Southern Ocean south of 47°S ($Gmolyr^{-1}$)
PI-control (pife1%)	3.47	0.092
70ka-control (pife1%)	3.47	0.092
lambfe1%	9.072	0.461
lambfe3%	27.44	1.383
lambfe5%	45.73	2.305
lambfe7%	64.02	3.227
lambfe10%	91.46	4.610
lambfe20%	182.9	9.221
glacfe1%	6.532	0.4425
glacfe3%	19.6	1.328
glacfe10%	65.32	4.425
glacfe20%	139.1	8.850
lambfe10%-30S	18.51	4.610
lambfe10%-40S	13.94	4.610
lambfe10%-50S	6.05	2.66
lambfe10%-60S	3.9	0.5
lambfe50%-47S	27.09	23.05
pife3%	10.41	0.27
pife5%	17.35	0.46
pife7%	24.29	0.64
pife10%	34.7	0.92
pife20%	69.4	1.84

Table2: ΔCO_2 for the sensitivity experiments compared to 70 ka-control, globally averaged P* values, as well as NPP and EP values integrated over different regions of the Southern Ocean. Percentage changes from 70ka-control experiment are provided in brackets.

Experiment	Change in CO_2 (ppm)	Global P*	SO NPP (30°S:90°S, $Pg\,Cyr^{-1}$)	SO NPP north of 47°S ($Pg\,Cyr^{-1}$)	SO NPP south of 47°S ($Pg\,Cyr^{-1}$)	SO EP (30°S:90°S, $Pg\,Cyr^{-1}$)	SO EP north of 47°S ($Pg\,C\,yr^{-1}$)	SO EP south of 47°S ($Pg\,C\,yr^{-1}$)
PI-control (pife1%)	-	0.515	14.63	7.62	7	3.84	1.58	2.267
70ka-control (pife1%)	0	0.553	13.52	5.38	8.15	3.76	1.13	2.63
lambfe1%	-3.8	0.566	13.58 (+0.4%)	4.55 (-15%)	9.04 (+11%)	3.93 (+4.5%)	0.99 (-12%)	2.93 (+11.6%)
lambfe3%	-8.9	0.590	13.43 (-0.6%)	3.77 (-30%)	9.68 (+18.7%)	4.08 (+8.6%)	0.84 (-25%)	3.23 (+23%)
lambfe5%	-11.4	0.602	13.36 (-1.1%)	3.47 (-35%)	9.89 (+21%)	4.14 (+10.3%)	0.79 (-30%)	3.36 (+30%)
lambfe7%	-13.5	0.611	13.31 (-1.5%)	3.31 (-38%)	10.02 (+23%)	4.19 (+11.4%)	0.75 (-33%)	3.44 (+30.7%)
lambfe10%	-15.3	0.621	13.27 (-1.8%)	3.16 (-41%)	10.12 (+24%)	4.22 (+12.4%)	0.72 (-36%)	3.5 (+33%)
lambfe20%	-18.7	0.634	13.35 (-1.2%)	3.01 (-44%)	10.35 (+27%)	4.33 (+15%)	0.68 (-39%)	3.64 (+38.5%)
glacfe1%	-5.1	0.574	13.39 (-0.9%)	4.43 (-17.6%)	8.97 (+10%)	3.92 (+4.3%)	0.97 (-13.7%)	2.94 (+12%)
glacfe3%	-10.7	0.599	13.21 (-2.2%)	3.60 (-33%)	9.62 (+18%)	4.07 (+8.2%)	0.81 (-28%)	3.25 (+23.8%)
glacfe10%	-16.3	0.628	13.14 (-2.8%)	3.12 (-42%)	10.03 (+23%)	4.20 (+11.7%)	0.71 (-37%)	3.5 (+32.8%)
glacfe20%	-18.9	0.642	13.09 (-3.1%)	2.98 (-45%)	10.12 (+24%)	4.25 (+13%)	0.68 (-40%)	3.57 (+36%)

Table3: ΔCO_2 simulated by changing the iron mask from PI to glacial (lambfe and glacfe) at 70ka BP but keeping the solubility constant.

Solubility	CO_2 anomaly (lambfe-pife)	CO_2 anomaly (glacfe-pife)
1%	-3.8	-5.1
3%	-6.4	-8.2
5%	-6.9	-
7%	-7.5	-
10%	-7.3	-8.3
20%	-6.7	-6.9

The difference in results between using either of the two glacial dust flux estimates that you apply in your experiments appears to give a weaker response than changing the solubility. This is an important result, which means that the global carbon cycle is more sensitive to factor changes in soluble iron flux that to differences in the horizontal flux pattern. It would be a good idea to discuss the result in the paper.

We thank the reviewer for this comment. Indeed, the changes in solubility factor have a larger impact on atmospheric CO_2 than the dust flux pattern in the Southern Ocean. We have indicated this result in L. 190-195. We also include this in the discussion as below:

Lines 345-348:

Despite these differences in spatial patterns, the two iron masks (glacfe and lambfe) with the same iron solubilities lead to similar decreases in atmospheric CO_2 in our simulations. This indicates that changes in atmospheric CO_2 are more dependent on changes in solubility, than on regional differences in aeolian iron fluxes in the Southern Ocean.

One of the novelties of the methodology is that it includes four functional types of phytoplankton: Normal phytoplankton, diazotrophs, coccolithofores, and diatoms. But how much does the inclusion of the new functional types affect the CO2 drop in the Southern Ocean fertilization experiments? In other words, how do the results of Saini et al. compare with a model with only regular phytoplankton and diazotrophs? It would be a benefit to the scientific community to have that comparison documented, since it would give us a hint on how necessary it is to include more planktic functional types in glacia-interglacial experiments.

We agree with the reviewer's comment that it is important to understand how the inclusion of different functional types of phytoplankton impacts the atmospheric CO_2 decrease. Lines 350-361 include a discussion of our results in comparison with previous modelling studies, which use different biogeochemical models. It should however be noted that all these previous modelling studies, except Menviel et al., 2012, were performed under different climate boundary conditions. Due to the different climate models and different boundary conditions, the climate changes differ among the simulations, thus making it challenging to isolate the impacts of the inclusion of different plankton classes. Nevertheless, we have now added the below paragraph:

Lines 381-387

None of the previous modelling studies simulate coccolithophores and diatoms' abundances prognostically. By including four distinct classes of plankton in our model we highlight the competitive dynamics between different major phytoplankton functional types for light and nutrient availability. Coccolithophores contribute to the total carbon export mainly in the polar frontal zone, while diatoms' contribution is in the Antarctic zone. As previously mentioned, carbon export close to convection sites in the Southern Ocean can be more efficient in reducing atmospheric CO_2. Furthermore, while both diatom and coccolithophores contribute to CO_2 uptake in the ocean through photosynthesis, coccolithophores produce $CaCO_3$ rich platelets, which reduce surface ocean alkalinity, thus reducing the CO_2 uptake efficiency.

What's the CO2 difference between your 70 ky and preindustrial experiments? I imagine it is higher in the 70 ky experiment due to lower global EP. Is that effect overcompensated by the Southern Ocean fertilization effect? It would be important to note this in the paper, since in the real climatr system the onset of the glaciation included physical changes as well as the assumed iron fertilization.

Both 70ka-control and PI runs were equilibrated with constant (forced) CO_2 values. The CO_2 is set at 289.5 ppm for PI and at 222.5 ppm for 70 ka based on the composite of Antarctic ice core estimates (Bereiter et al., 2015). Once the carbon cycle equilibrated to these imposed CO_2 concentrations, we calculated CO_2 prognostically for a few hundred years, to ensure that there is no remaining drift. While it would be interesting to study the impact of climate change on the 70ka CO_2 level, this is out of the scope of the present study.

Another novelty of the model is the inclusion of a sediment model, which allows changes in global alkalinity. Does global alkalinity vary significantly among your experiments? Does the variation in CO2 that you find depend on global alkalinity changes at all? This is a topic that could be potentially addressed in this paper.

We thank the reviewer for this comment and agree that changes in oceanic alkalinity can significantly impact atmospheric CO_2. However, in our experimental setup, the river inflow compensates for the $CaCO_3$ burial to keep global alkalinity constant. This was a choice we made at the beginning of this project, and although we agree that this would be an interesting question to explore, we cannot do so with our simulations.

Minor comments:

Line 19: No need for the ~ symbol if you include uncertainty.

Incorporated throughout the text.

Line 121: What leads? The sentence is not clear.

The lambfe aeolian iron input south of 47S with a 50% solubility is equivalent to 23.05 Gmol/yr iron input. The sentence is now modified as:

Lines 148-150:

In the fifth sensitivity experiment (lambfe50%-47S), the aeolian iron input south of 47°S follows the lambfe mask with a solubility factor of 50% (Figure A1f), which is equivalent to 23.05 $Gmolyr^{-1}$ iron input in the Southern Ocean south of 47°S and provides an upper limit on the potential CO_2 draw-down.

Fig. 2: Color scale poorly chosen, it saturates in most places.

We apologise for the poor choice of colour scale. Figure 2 in the manuscript is now modified and shown as Fig. R2 below:

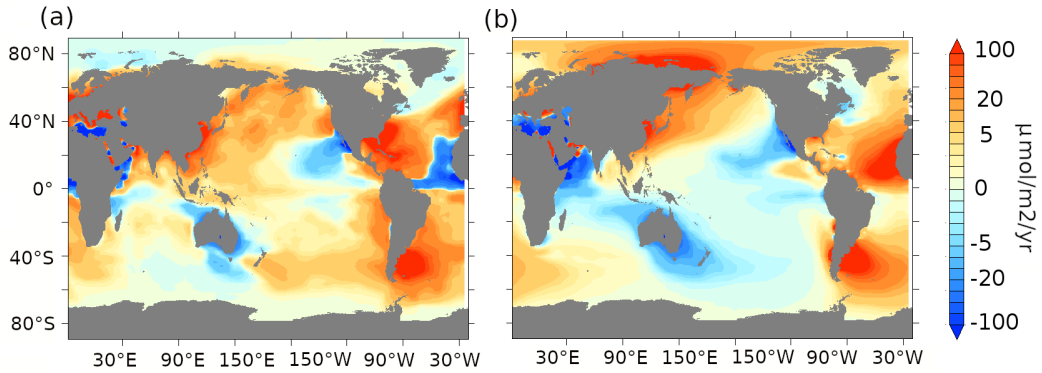

Fig.R2: Aeolian iron dust flux (µmol m^{-2} yr^{-1}) anomalies for (a) lambfe1% minus pife1% and (b) glacfe1% minus pife1%.

Fig. 3: Why does the North Altantic show such a complex pattern of EP anomalies? Is it changes in convection, ventilation, the AMOC?

Yes, the complex changes are due to shifts in convection sites in the North Atlantic. A main convection site south of Iceland in our PI simulation shifted to the east (please refer to fig. below), leading to lower diatom and higher coccolithophore populations at this location and an increase in diatoms in the eastern North Atlantic. In the west, near the coast of Nova Scotia, both diatoms and coccolithophores increase.

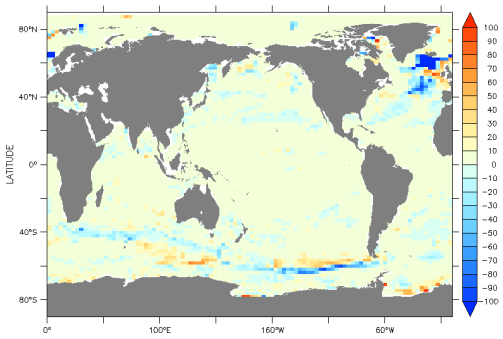

Fig.R3: Ventilation depth (m) anomalies for 70ka-control compared to PI.

The following text is added as below:

Lines 187-188

The North Atlantic shows a complex pattern of anomalies due to changes in the strength and location of deep ocean convection, which result in an overall decrease in NPP and EP by 16% and 9%, respectively.

Fig. 4d shading colors not easily distinguishable. Why does terrestrial carbon go down in your simulations?

We have modified the colour scale of Figure 4d (as also shown in Fig.R1 above).

As the iron input to the ocean increases, so does the efficiency of the biological pump, which leads to an increase in the oceanic carbon reservoir and thus an atmospheric CO_2 decrease. The atmospheric CO_2 decrease in turn leads to a cooling, and overall drier conditions over land. This climate change reduces the terrestrial carbon reservoir, with contributions from both soil and vegetation carbon.

This explanation is given in lines 255-259:

The simulated decrease in atmospheric CO_2, equivalent to 8-45 GtC (Figure 4d, red shade), leads to a decrease in surface air temperatures, as well as regional changes in precipitation and soil moisture. In addition, the lower atmospheric CO_2 concentration also reduces photosynthesis and consequently litter fall. The direct and indirect effects of a lower atmospheric CO_2 concentration result in a terrestrial carbon decrease of 16 to 88 GtC (Figure 4d, green shade), out of which 8 to 45 GtC decrease is from terrestrial vegetation while 8 to 43 GtC reduction is from soil carbon.

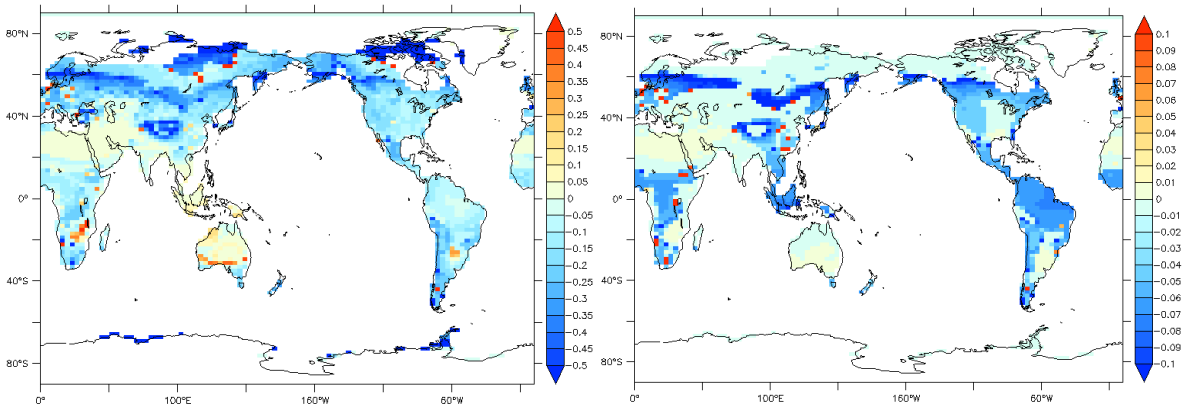

Fig R4: Soil (left) and vegetation (right) carbon (g/m2) anomalies for lambfe3% compared to 70ka-control.

The global iron flux in experiments lambfe10% and lambfe3% is not shown anywhere. The fluxes should be plotted somewhere in the paper, since the results of these simulations are discussed in detail.

We apologise for this missing information. In Fig.2 in the manuscript, we show the lambfe and glacfe 1% dust fluxes compared to pife 1% flux. For completeness we now also show pife, lambfe, glacfe iron fluxes with 3% and 10% solubility. The fluxes are now added in the supplementary as Figure A2.

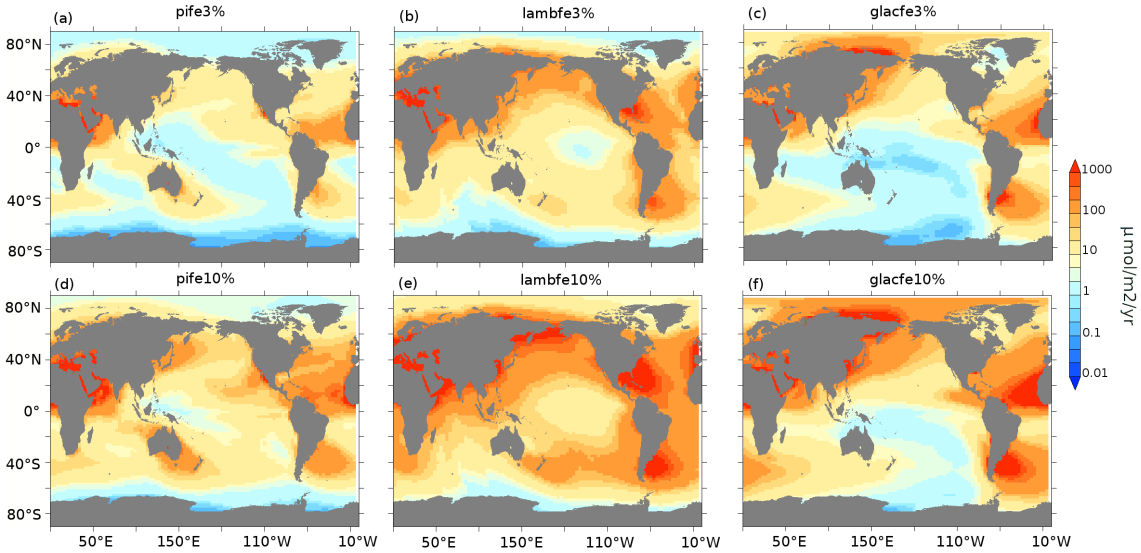

Fig. R5: Aeolian iron dust fluxes (μmol m^{-2} yr^{-1}) for pife (a,d), lambfe (b,e) and glacfe (c,f) masks with 3% (top row) and 10% (bottom row) solubility factors.